Chapter 10

Slanted waves

In this final chapter of the book are gathered together imaging concepts that have been published, but have not yet come into routine industrial use. The first part of this chapter develops the mathematical concept of linear moveout and how it relates to velocity analysis. Data can be focused so that the interval velocity can be read directly. The latter part of the chapter is about multiple reflections. Here too linear moveout helps to define the problem. You will see basic mathematical tools that have the power to deal with multiple reflections and lateral velocity variations. This chapter has many data processing proposals. They are not descriptions of production processes!

10.0.1 Interpreting seismic data

Initially I regarded this chapter as one for specialists interested mainly in devising new processes. Then I realized that in dealing with things that don't seem to work as they are expected to, we are really, for the first time, struggling to contend with reality, not with what theory predicts. This can hold much interest for skilled interpreters.

The heart of petroleum prospecting is the interpretation of reflection seismic data. What is seismic interpretation? To be a "routine interpreter" you must know everything on which theory and practice generally agree. To be a *good* interpreter you must know the "noise level" of alternate phenomena with similar effects. Anomalies in seismic data can arise from the complexity of the earth itself, from seismic wave propagation in the earth (deep, near surface, or out of plane), or from imperfections in recording and imaging techniques. To make realistic judgements in so wide a realm, you must be a seismologist who is part geologist, part engineer, and part mathematician. This chapter will not teach you to be a good interpreter, but it will offer you a chance to observe some critical thinking about the relationship of seismic theory to seismic data.

10.0.2 Leaning

Echo delay is much like depth. We usually measure angles by their departure from the *vertical* ray, while in reality zero-offset data is rarely recorded. The best seismic data is usually far from vertical. In this chapter a pattern of thinking is developed that is oriented about a selected nonvertical ray. Rotation of coordinates does not solve the problem since after rotation, the plane on which measurements would be made would no longer be simply $z = 0$. Rotation would also make a mess of the simple seismic velocity function $v(z)$ by making it a strongly two-dimensional function $v'(x', z')$. The view of offset presented in chapter 6 may have seemed rather complete, but in fact it was not very general because square roots were expanded about the vertical ray. The Stolt stretch illustrated the advantage of leaving the hyperbola top and getting out on the flanks.

Linear moveout (LMO) is the way to reorient our thinking about nonvertical rays. While not widely incorporated in the modern production environment, this deeper view of offset is of special interest to researchers. It offers an understanding of multiple reflections, a subject untouched in chapter 6. It also offers a better understanding of velocity estimation.

10.0.3 Stepout review

Earlier a *Snell* wave was defined as a plane wave that has become nonplanar by moving into a velocity-stratified medium $v = v(z)$. A plane wave keeps its angle of propagation constant, while a Snell wave keeps its stepout dt/dx a constant function of z. Figure 1.1 shows a Snell wave incident on the earth's surface. The wavefronts

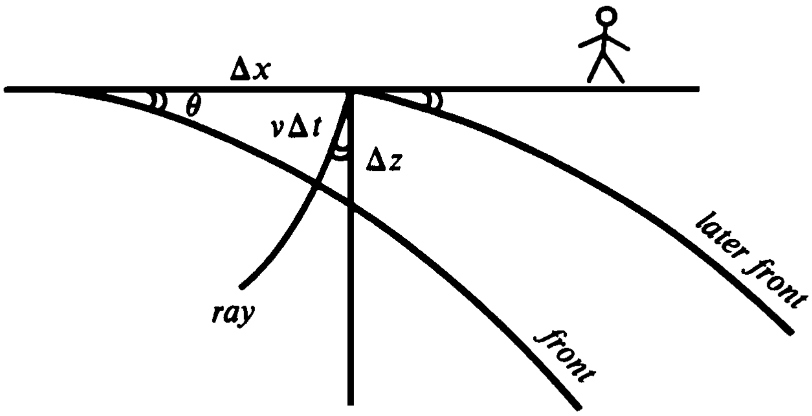

Figure 10.1: Wavefront arrival at earth's surface, showing that observation of dt/dx gives the ratio $dt/dx = (\sin\theta)/v$. slnt-fronts [NR]

at successive times are not parallel to each other; they are horizontal translations of one another. The *slowness* of horizontal motion is called the *stepout*. It is measured in units of inverse velocity and is given as milliseconds per meter or as seconds per kilometer. The slowness, denoted as p, is also called the *ray parameter* or the *Snell parameter:*

$$p \quad = \quad \frac{dt}{dx} \quad = \quad \frac{\sin\,\theta(z)}{v(z)} \quad = \quad \text{const}(z) \tag{10.1}$$

10.1 RADIAL TRACES

Radial trace sections were introduced as an alternative to constant-offset sections. Previously the goal was to achieve a proper migration of nonzero-offset data. We also saw the definition of dip moveout (DMO). DMO simplifies further analysis because after DMO we can analyze gathers assuming that they come from a horizontally layered earth.

A *radial trace gather* is defined by a deformation of an ordinary gather. Let the ordinary gather be denoted by $P(x,t)$. Let the radial parameter be denoted by $r = x/t$. Then the radial trace gather $P'(r,t)$ is defined by the deformation $P'(r,t) = P(rt,t)$.

The horizontal location x of the tip of a ray moves according to $x = vt\sin\theta$. So in a constant-velocity medium, the radial trace with a fixed $r = x/t$ contains all the energy that propagates at angle θ.

The constancy of propagation angle within a radial trace should be helpful in the analysis of multiple reflections. It should also be helpful in compensation for the shot waveform, since the antenna effects of the shot and geophone arrays are time-invariant on each radial trace.

Assuming reflectors at depth z_j and constant velocity, hyperbolic travel-time curves are

$$t^2\,v^2 \quad = \quad x^2 \;+\; z_j^2 \tag{10.2}$$

Let us see what happens to the hyperbola (1.2) when the offset x is transformed to the radial parameter $r = x/t$. We get an equation for a family of curves in the (r,t)-plane (plotted in Figure 1.2.

$$z_j^2 \quad = \quad t^2\;(v^2 \;-\; r^2) \tag{10.3}$$

The asymptotes, instead of being along sloping lines $x^2 = \pm v^2 t^2$, are along vertical lines $r = \pm v$. The filled region of the (r,t)-plane is rectangular, while the filled region of the (x,t)-plane is triangular.

Figure 1.3 shows a field profile before and after transformation to radial space. Zero traces were interspersed between live ones to clarify the shape of the deformation. To understand this deformation, it helps to remember that a field trace is a curve of constant $x = rt$.

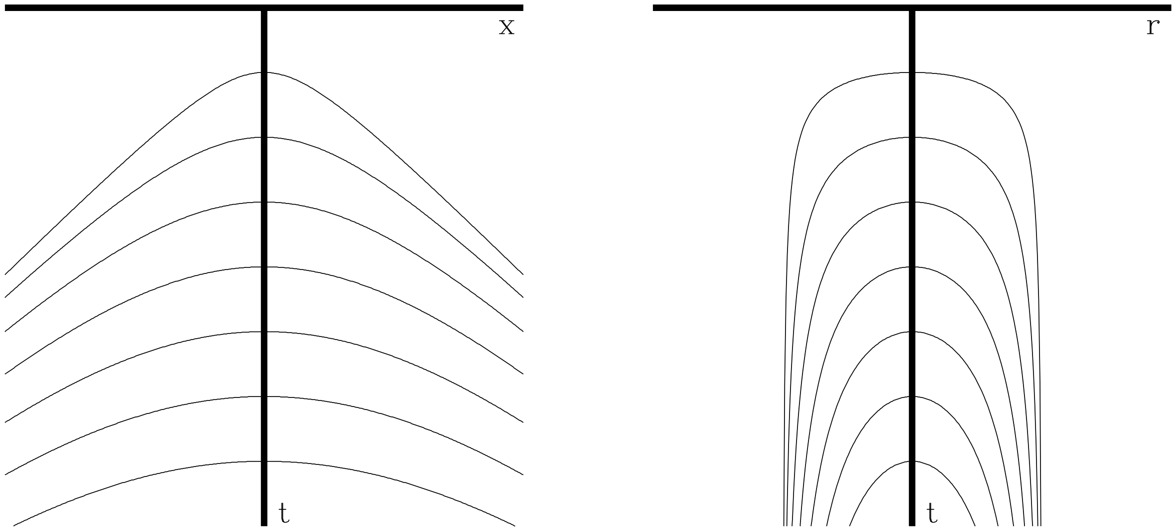

Figure 10.2: Family of hyperbolas before and after transformation to radial space. slnt-radial1 [ER]

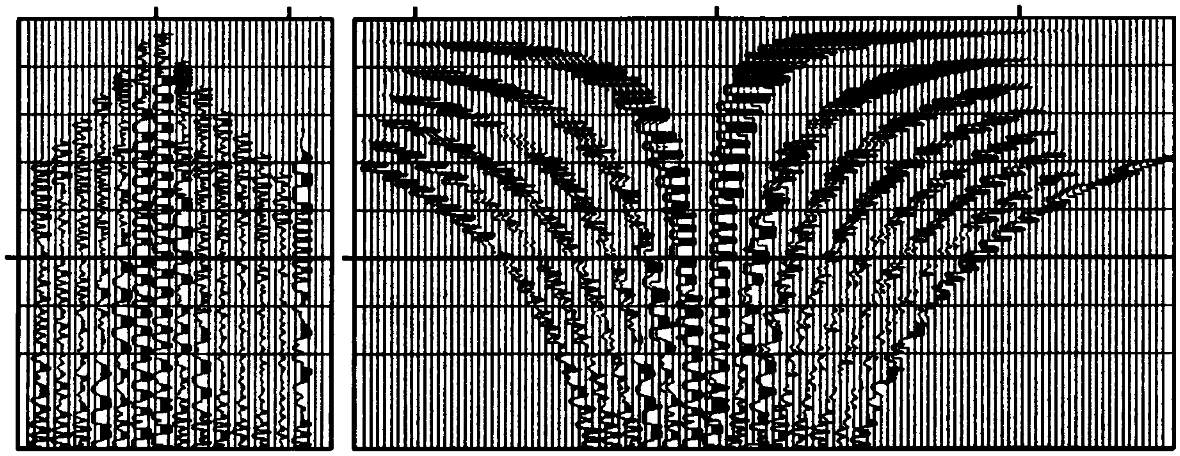

Figure 10.3: Field profile from Alberta (Western Geophysical) interspersed with zero traces, shown before and after radial-trace deformation. slnt-radial2 [NR]

An interesting aspect of the radial-trace transformation is its effect on ground roll. A simple model of ground roll is a wave traveling horizontally at a constant rate. So on a radial-trace gather the ground roll is found as d.c. (zero frequency) on a few radial traces near $r = \pm v_{\text{roll}}$. Figure 1.4 shows an approximation to the idealization.

10.1.1 Moveout-corrected radial traces

Moveout correction may be regarded as a transformation from time to depth. When the moveout correction is properly done, all traces should show the same depth-dependent reflectivity. In principle, radial moveout correction proceeds by introducing z and eliminating t with the substitution $tv = \sqrt{z^2 + x^2}$. In practice you would prefer a travel-time-depth axis to a depth axis. So the transformation equation becomes $t = \sqrt{\tau^2 + x^2/v^2}$. Eliminating x with rt we get

$$t \quad = \quad \frac{\tau}{\sqrt{1 \ - \ r^2/v^2}} \tag{10.4}$$

Inspecting (1.4) we see that moveout correction in radial-trace coordinates is a *uniform compression* of the time t-axis into a τ-axis. The amount of compression is fixed when r is fixed. The amount of compression does not change with time. The uniformity of the compression is an aid to modeling and removing the effects of shot waveforms and multiple reflections. It is curious to note that moveout correction of radial traces *compresses* time, while moveout correction of constant-offset data *stretches* time nonuniformly. Figure 1.4 shows a field profile before and after the radial-trace transformation.

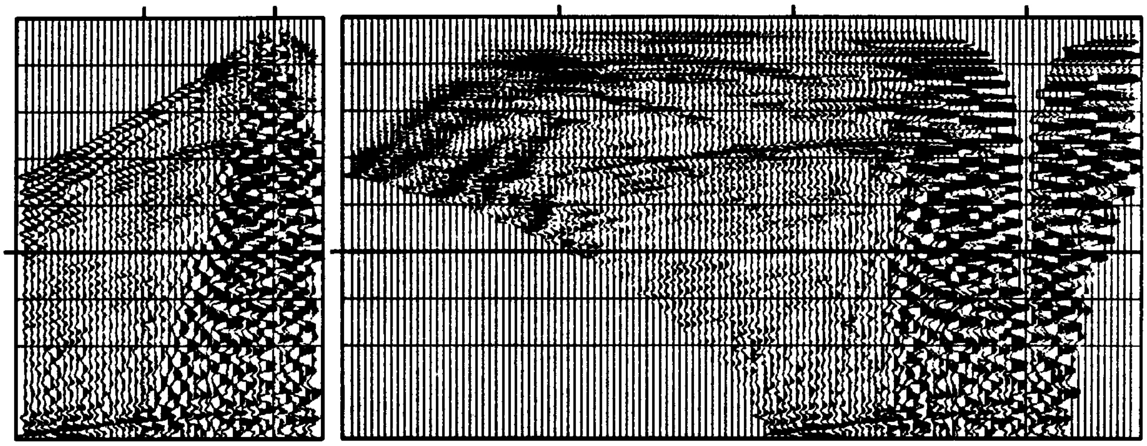

Figure 10.4: Field profile from Alberta (Western Geophysical) shown before and after deformation into radial traces. slnt-radial3 [NR]

10.1.2 Snell traces

the radial-trace coordinate system can be used no matter what the velocity of the earth. But the coordinate system has a special advantage when the velocity is constant, because then it gathers all the energy of a fixed propagation angle. The logical generalization to stratified media is to gather all the energy with a fixed Snell parameter. A *Snell trace* is defined (Ottolini) as a trajectory on the (x,t)-plane where the stepout $p = dt/dx$ would be constant if the velocity were $v(z)$. Where the velocity increases with depth, the Snell traces bend upward. The Snell trace trajectory is readily found by integrating the ray equations:

$$x = \int_0^z \tan\theta \, dz \tag{10.5}$$

$$t = \int_0^z \frac{dz}{v \cos\theta} \tag{10.6}$$

To do moveout correction on the Snell traces, introduce the vertical travel-time depth t such that $dz = v d\tau$. The radial-trace moveout-correction equations become

$$x(p,\tau) = \int_0^\tau \frac{p\,v^2}{\sqrt{1-p^2v^2}} \, d\tau \tag{10.7}$$

$$t(p,\tau) = \int_0^\tau \frac{1}{\sqrt{1-p^2v^2}} \, d\tau \tag{10.8}$$

Where the earth velocity is stratified, Snell traces have a theoretical advantage over radial traces. However they have the disadvantage that the curves could become multibranched, so that the transformation would not be one-to-one. So in practice you might use a simplified velocity model instead of your best estimate of the true velocity.

More philosophically, the transition from constant-offset traces to radial traces is a big one, whereas the transition from radial traces to Snell traces is not so large. Since the use of radial traces is not widespread, we can speculate that the practical usefulness of Snell traces may be further limited.

10.2 SLANT STACK

Slant stack is a transformation of the offset axis. It is like steering a beam of seismic waves. I believe I introduced the term *slant stack* (Schultz and Claerbout [1978]) as a part of a migration method to be described next. I certainly didn't invent the slant-stack concept! It has a long history in exploration seismology going back to Professor Rieber in the 1930s and to Professor Riabinkin in the Soviet Union. Mathematically, the slant-stack concept is found in the Radon [1917] transformation.

The slant-stack idea resembles the Snell trace method of organizing data around emergent angle. The Snell trace idea selects data based on a hypothetical velocity predicting the local stepout $p = dt/dx$. Slant stack does not *predict* the stepout, but *extracts* it by filtering. Thus slant stack does its job correctly whether or not the velocity is known. When the velocity of the medium is known, slant stack enables immediate downward continuation even when mixed apparent velocities are present as with diffractions and multiple reflections.

10.2.1 Slant stacking and linear moveout

Looking on profiles or gathers for events of some particular stepout $p = dt/dx$ amounts to scanning hyperbolic events to find the places where they are tangent to a straight line of slope p. The search and analysis will be easier if the data is replotted with *linear moveout*—that is, if energy located at offset $x = g - s$ and time t in the (x, t)-plane is moved to time $\tau = t - px$ in the (x, τ)-plane. This process is depicted in Figure 1.5. The linear moveout converts all events stepping out at a rate p in (x, t)-

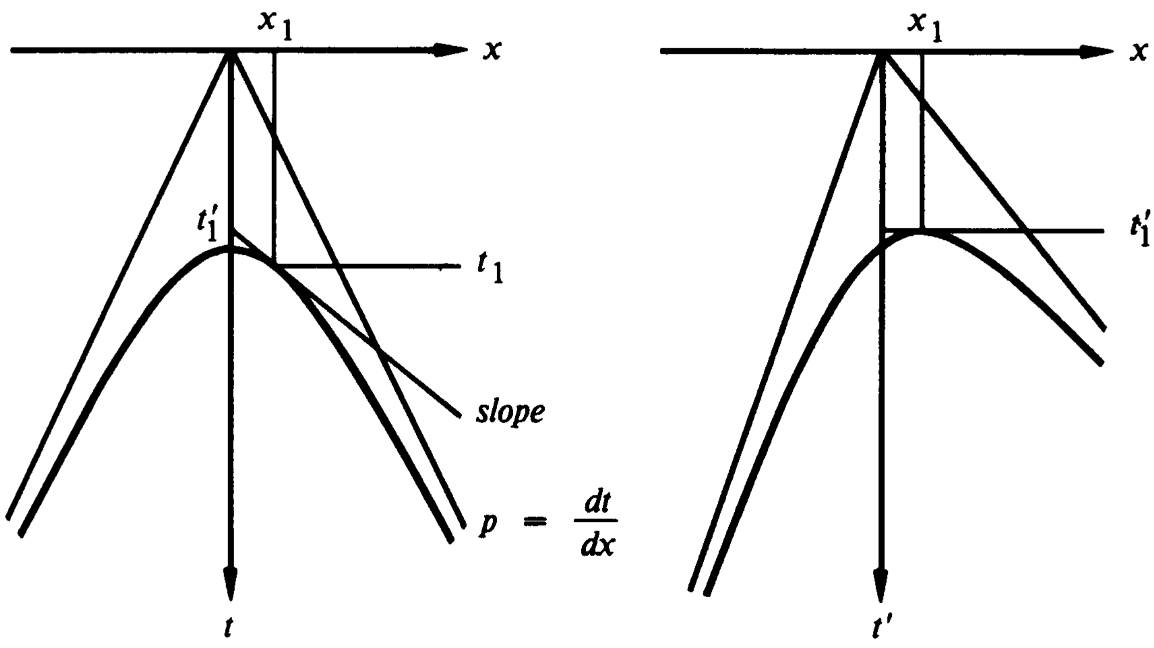

Figure 10.5: Linear moveout converts the task of identifying tangencies to constructed parallel lines to the task of locating the tops of convex events. slnt-lmo [NR]

space to "horizontal" events in (x, τ)-space. The presence of horizontal timing lines facilitates the search for and the identification and measurement of the locations of the events.

After linear moveout $\tau = t - px$, the components in the data that have Snell parameters near p are slowly variable along the x'-axis. To extract them, apply a low-pass filter on the x'-axis, and do so for each value of τ. The limiting case of low-frequency filtering is extracting the mean. This leads to the idea of slant stack.

To *slant stack* , do linear moveout with $\tau = t - px$, then sum over x'. This is the same as summing along slanted lines in (t, x)-space. In either case, the entire gather $P(x, t)$ gets converted to a single trace that is a function of τ.

Slant stack assumes that the sum over observed offsets is an adequate representation of integration over all offset. The (slanted) integral over offset will receive its major contribution from the zone in which the path of integration becomes tangent to the hyperboloidal arrivals. On the other hand, the contribution to the integral is vanishingly small when the arrival-time curve crosses the integration curve. The reason is that propagating waves have no zero-frequency component.

The strength of an arrival depends on the length of the zone of tangency. The Fresnel definition of the length of the zone of tangency is based on a half-wavelength condition. In an earth of constant velocity (but many flat layers) the width of the tangency zone would broaden with time as the hyperbolas flatten. This increase goes as $\sqrt{t}$, which accounts for half the spherical-divergence correction. In other words, slant stacking takes us from two dimensions to one, but a $\sqrt{t}$ remains to correct the conical wavefront of three dimensions to the plane wave of two.

10.2.2 Slant-stack gathers are ellipses

A slant stack of a data gather yields a single trace characterized by the slant parameter p. Slant stacking at many p-values yields a *slant-stack gather.* (Those with a strong mathematical-physics background will note that slant stacking transforms travel-time curves by the Legendre transformation. Especially clear background reading is found in *Thermodynamics,* by H.B. Callen, Wiley, 1960, pp. 90-95).

Let us see what happens to the familiar family of hyperbolas $t^2v^2 = z_j^2 + x^2$ when we slant stack. It will be convenient to consider the circle and hyperbola equations in *parametric* form, that is, instead of $t^2v^2 = x^2 + z^2$, we use $z = vt\cos\theta$ and $x = vt\sin\theta$ or $x = z\tan\theta$. Take the equation for linear moveout

$$\tau \quad = \quad t \;-\; p\,x \tag{10.9}$$

and eliminate t and x with the parametric equations.

$$\tau \quad = \quad \frac{z}{v\,\cos\theta} \;-\; \frac{\sin\theta}{v}\; z\,\tan\theta \quad = \quad \frac{z}{v}\,\cos\theta \tag{10.10}$$

$$\tau \quad = \quad \frac{z}{v}\sqrt{1 \;-\; p^2v^2} \tag{10.11}$$

Squaring gives the familiar ellipse equation

$$\left(\frac{\tau}{z}\right)^2 \;+\; p^2 \quad = \quad \frac{1}{v^2} \tag{10.12}$$

Equation (1.12) is plotted in Figure 1.6 for various reflector depths z_j.

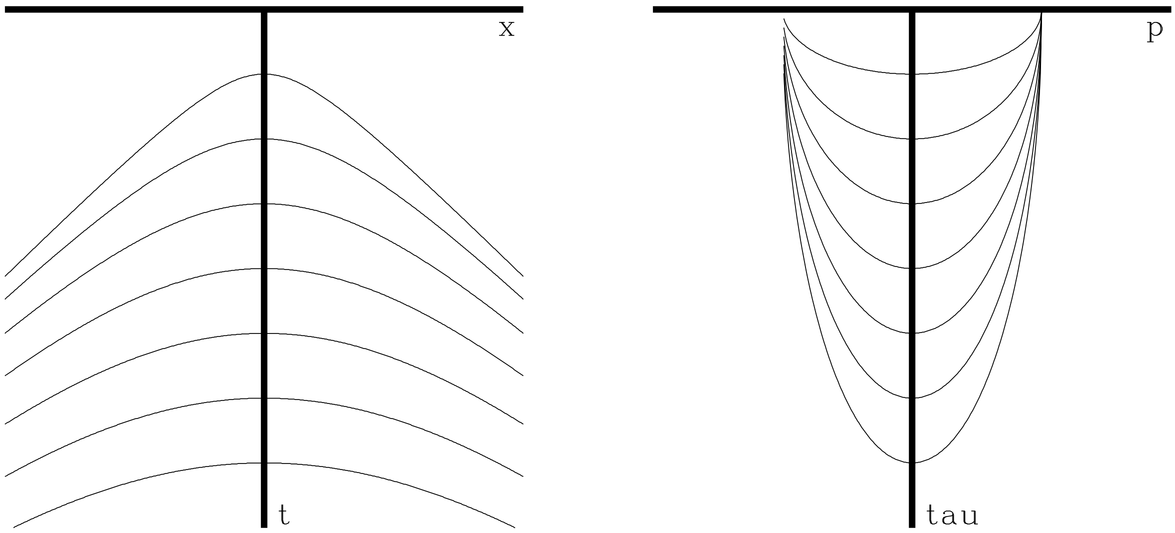

Figure 10.6: Travel-time curves for a data gather on a multilayer earth model of constant velocity before and after slant stacking. slnt-sstt [ER]

10.2.3 Two-layer model

Figure 1.7 shows the travel times of waves in a two-layer model. As is the usual case,

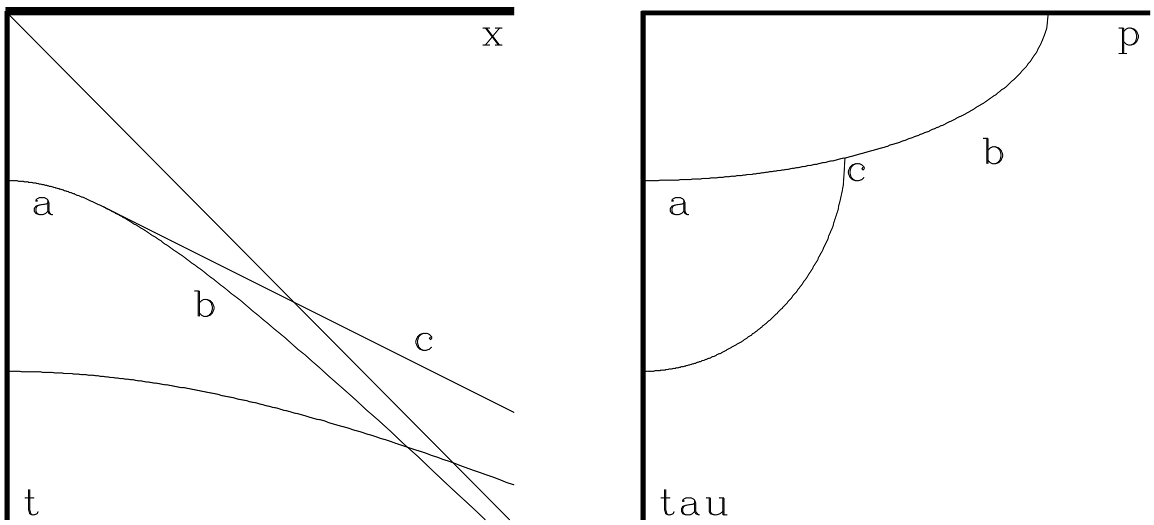

Figure 10.7: Identification of precritical reflection (a), postcritical reflection (b), and head wave (c). slnt-sslayer [ER]

the velocity is higher in the deeper layer. At the left are the familiar hyperboloidal curves. Strictly, the top curve is exactly a hyperbola whereas the lower curve is merely hyperboloidal. The straight line through the origin represents energy traveling horizontally along the earth's surface. The lower straight line is the head wave. (In seismology it is often called the *refracted* wave, but this name can cause confusion).

It represents a ray that hits the deeper layer at critical angle and then propagates horizontally along the interface.

The right side of the figure shows the travel-time curves after slant stacking. Note that curves cross one another in the (x, t)-space but they do not cross one another in the (p, τ)-space. The horizontal axis $p = dt/dx$ has physical dimensions inverse to velocity. Indeed, the velocity of each layer may be read from its travel-time curve as the maximum p-value on its ellipse. The head waves—which are straight lines in (x, t)-space—are points in (p, τ)-space located where the ellipsoids touch. The top curve in (p, τ)-space is exactly an ellipse, and the lower curve is merely ellipsoidal.

10.2.4 Interval velocities from slant stacks

Earlier we showed that downward continuation of Snell waves is purely a matter of time shift. The amount of time shift depends only on the angle of the waves. For example, a frequency domain equation for the shifting is

$$P(\omega, p, z_2) \quad = \quad P(\omega, p, z_1)\; e^{-i \frac{\omega}{v} \sqrt{1 \;-\; p^2 v^2}\;(z_2 \;-\; z_1)} \tag{10.13}$$

Downward continuing to the first reflector, we find that the first reflections should arrive at zero time. In migration it is customary to retard time with respect to the zero-dip ray. So downward continuation in retarded time flattens the first reflection without changing the zero-dip ray. Time shifting the data to align on the first-layer reflection is illustrated by the third panel in Figure 1.8. The first panel shows the velocity model, and the second panel shows the slant stacks at the surface. After the first reflector is time aligned, we have the data that should be observed at the bottom of the first layer. Now the next deeper curve is an exact ellipse. Estimate the next deeper velocity from that next deeper ellipse. Continue the procedure to all depths. This method of velocity estimation was proposed and tested by P. Schultz [1982].

Figure 1.8 illustrates the difficulty caused by a shallow, high-velocity layer. Reflection

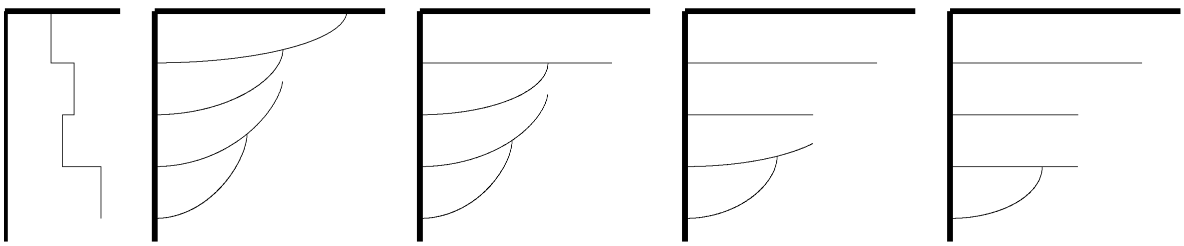

Figure 10.8: Schultz flattening on successive layers. slnt-schultz [ER]

from the bottom of any deeper, lower-velocity layer gives an incomplete ellipse. It does not connect to the ellipse above because it seems to want to extend beyond. The large p-values (dotted in the figure) are missing because they are blocked by the high-velocity (low p) layer above. The cutoff in p happens where waves in the high-velocity layer go horizontally. So there are no head waves on deeper, lower-velocity layer bottoms.

Schultz's method of estimating velocity from an ellipse proceeds by summing on scanning ellipses of various velocities and selecting the one with the most power. So his method should not be troubled by shallow high-velocity layers. It is interesting to note that when the velocity does increase continuously with depth, the velocity-depth curve can be read directly from the rightmost panel of Figure 1.8. The velocity-depth curve would be the line connecting the ends (maximum p) of the reflections, i.e. the head waves.

10.2.5 Interface velocity from head waves

The determination of earth velocity from head waves is an old subject in seismology. Velocity measurement from head waves, where it is possible, refers to a specific depth—the depth of the interface—so it has even better depth-resolving power than an *interval* velocity (the velocity of a depth interval between two reflections).

Traditionally, head-wave velocity analysis involved identification (picking) of travel times. Travel times are hard to pick out on noisy data. Clayton and McMechan [1981] introduced a new method based on the wavefield itself, instead of on picked travel times. They did for the velocity analysis of head waves what wave-equation migration did for reflections.

The same idea for getting velocity from back-scattered head waves on sections can be used on ordinary head waves on common-midpoint gathers. On gathers you have the extra information not on a section that downward continuation focuses energy on zero offset. The focus is not a featureless point. Take original data to consist of a head wave only, with no reflection. Downward continuation yields a focus at zero offset. The focus is a concentrated patch of energy oriented with the same stepout dt/dh as the original unfocused head wave. Summing through the focus at all possible orientations (slant stack) transforms the data $u(h,\tau)$ to dip space, say $\bar{u}(p,\tau)$. The velocity of the earth at travel-time depth τ is found where the seismic energy has concentrated on the (p,τ)-plane. The velocity is given directly by $v(\tau) = 1/p(\tau)$. Given $v(\tau)$, $v(z)$ is readily found. Or the entire calculation could be done in depth z directly instead of in travel-time depth τ.

Clayton and McMechan actually do the downward continuation and the slant stack in the opposite order. They slant stack first and then downward continue. In principle these processes can be done in either order. Remember that we are bootstrapping to the correct earth velocity. Slant stacking does not depend on the earth's velocity, but downward continuation does. Slant stacking need be done only once if it is done first, which is why Clayton and McMechan do it that way. Figures 1.9 and 1.10 show one of their examples.

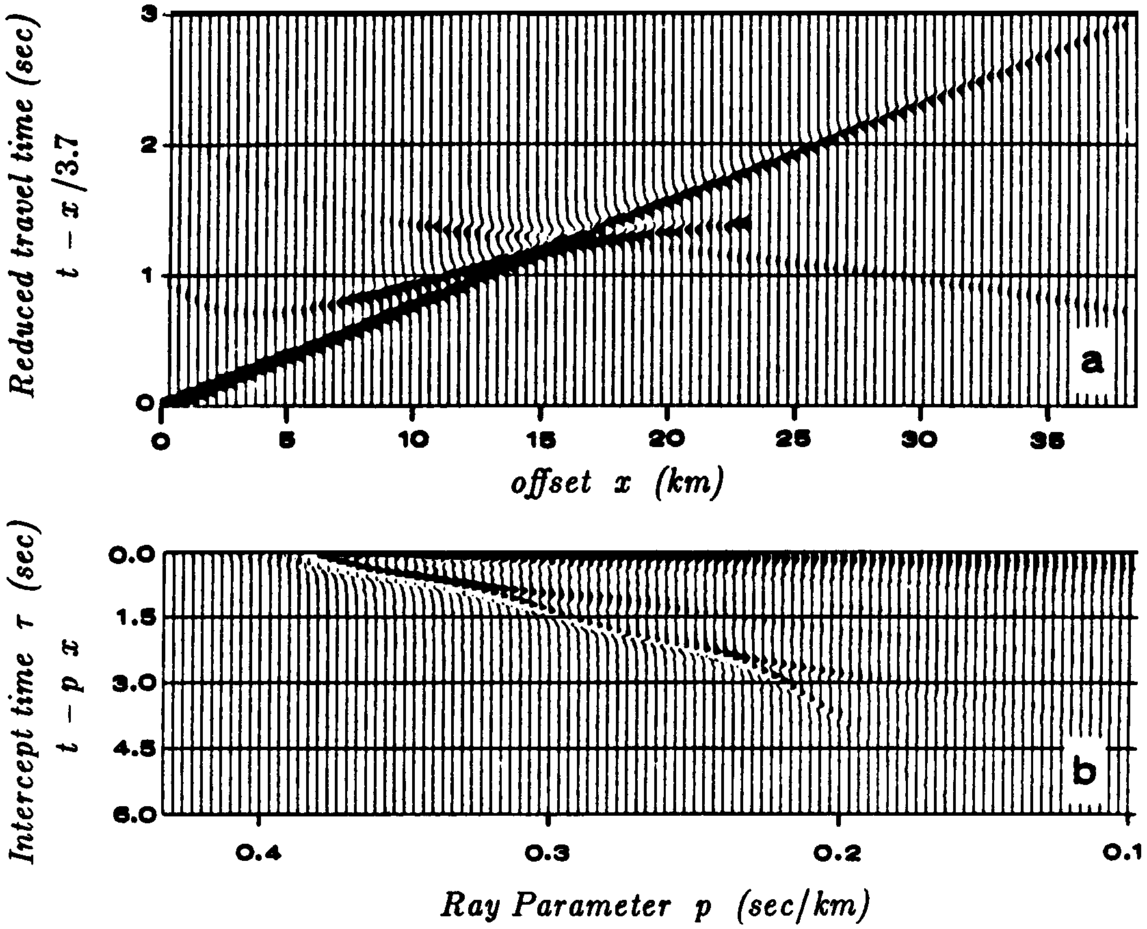

Figure 10.9: The upper figure (a) contains a synthetic head-wave profile (plotted with linear moveout). The data is transformed by slant stack to the lower half of the figure (b). The result of downward continuation of this slant-stacked wavefield (b) is shown in Figure 1.10. (Clayton & McMechan) slnt-sshead [NR]

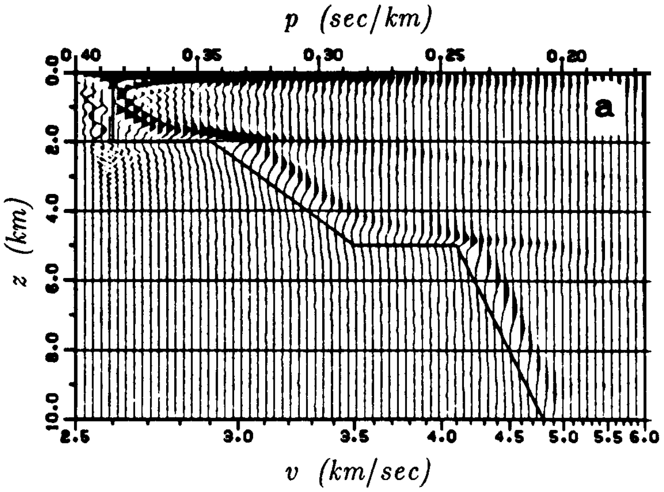

Figure 10.10: The result of downward continuation of the slant-stacked wavefield at the top of Figure 1.9 with the correct velocity-depth function (the solid line). (Clayton & McMechan) slnt-sshead2 [NR]

Compare the method of Clayton and McMechan to that of Schultz. Schultz flattens the reflections by a method that is sensitive to the large p parts of the ellipse. Clayton and McMechan look only at the largest p part of the ellipse. Schultz has the advantage that a method based on reflection is not troubled by high-velocity layers, but the disadvantage that decision making is required during the descent. Clayton and McMechan present the interpreter with a plane of information from which the interpreter selects the velocity. Clayton and McMechan's velocity space is a linear, invertible function of the data.

10.2.6 Slant stack and Fourier transform

Let $u(x,t)$ be a wavefield. The *slant stack* $\bar{u}(p,\tau)$ of the wavefield is defined mathematically by

$$\boxed{\overline{u}(p,\tau) = \int u(x, \tau + px)\ dx} \tag{10.14}$$

The integral across x in (1.14) is done at constant τ, which is a slanting line in the (x,t)-plane.

Slant stack is readily expressed in Fourier space. The definition of the two-dimensional Fourier transformation of the wavefield $u(x,t)$ is

$$U(k,\omega) \quad = \quad \int\int\ e^{i\omega t\,-\,ikx}\ u(x,t)\ dx\ dt \tag{10.15}$$

Recall the definition of Snell's parameter in Fourier space $p = k/\omega$ and use it to eliminate k from the 2-D Fourier transform (1.15).

$$U(\omega p,\omega) \quad = \quad \int\int\ e^{i\omega(t\,-\,px)}\ u(x,t)\ dx\ dt \tag{10.16}$$

Change the integration variable from t to $\tau = t - px$.

$$U(\omega p,\omega) \quad = \quad \int\ e^{i\omega\tau}\ [\ \int\ u(x,\tau\,+\,px)\ dx\ ]\ d\tau \tag{10.17}$$

Insert the definition (1.14) into (1.17).

$$U(\omega p,\omega) \quad = \quad \int\ e^{i\omega\tau}\ \bar{u}(p,\tau)\ d\tau \tag{10.18}$$

Think of $U(\omega p,\omega)$ as a one-dimensional function of ω that is extracted from the (k,ω)-plane along the line $k = \omega p$.

The inverse Fourier transform of (1.18) is

$$\boxed{\overline{u}(p,\tau) \ = \ \int e^{-i\omega\tau} U(\omega p,\omega)\ d\omega} \tag{10.19}$$

The result (1.19) states that a slant stack can be created by Fourier-domain operations. First you transform $u(x,t)$ to $U(k,\omega)$. Then extract $U(\omega p,\omega)$ from $U(k,\omega)$. Finally, inverse transform from ω to τ and repeat the process for all interesting values of p.

Getting $U(\omega p,\omega)$ from $U(k,\omega)$ seems easy, but this turns out to be the hard part. The line $k=\omega p$ will not pass nicely through all the mesh points (unless $p=\Delta t/\Delta x$) so some interpolation must be done. As we have seen from the computational artifacts of Stolt migration, Fourier-domain interpolation should not be done casually.

Both (1.14) and (1.19) are used in practice. In (1.14) you have better control of truncation and aliasing. For large datasets, (1.19) is much faster.

10.2.7 Inverse slant stack

Tomography in medical imaging is based on the same mathematics as inverse slant stack. Simply stated, (two-dimensional) tomography or inverse slant stacking is the reconstruction of a function given line integrals through it. The inverse slant-stack formula will follow from the definition of two-dimensional Fourier integration:

$$u(x,t) \quad = \quad \int e^{-i\omega t}\ [\int e^{ikx}\ U(k,\omega)\ dk\ ]\ d\omega \tag{10.20}$$

Substitute $k=\omega p$ and $dk=\omega\, dp$ into (1.20). Notice that when ω is negative the integration with dp runs from positive to negative instead of the reverse. To keep the integration in the conventional sense of negative to positive, introduce the absolute value $|\omega|$. (More generally, a change of variable of volume integrals introduces the *Jacobian* of the transformation). Thus,

$$u(x,t) \quad = \quad \int e^{-i\omega t}\ [\int e^{i\omega px}\ U(\omega p,\omega)\ |\omega|\ dp\ ]\ d\omega \tag{10.21}$$

$$u(x,t) \quad = \quad \int \int e^{-i\omega t}\ [\ U(\omega p,\omega)\ e^{i\omega px}\ |\omega|\ ]\ d\omega \quad dp \tag{10.22}$$

Observe that the { } in (1.22) contain an inverse Fourier transform of a product of three functions of frequency. The product of three functions in the ω-domain is a convolution in the time domain. The three functions are first $U(\omega p,\omega)$, which by (1.19) is the FT of the slant stack. Second is a delay operator $e^{i\omega px}$, i.e an impulse function of time at time px. Third is an $|\omega|$ filter. The $|\omega|$ filter is called a *rho* filter. The *rho* filter does not depend on p so we may separate it from the integration over p. Let "*" denote convolution. Introduce the delay px as an argument shift. Finally we have the inverse slant-stack equation we have been seeking:

$$\boxed{u(x,t) \ = \ rho(t)\ *\ \int \overline{u}(p,t-px)\ dp} \tag{10.23}$$

It is curious that the inverse to the slant-stack operation (1.14) is basically another slant-stacking operation (1.23) with a sign change.

10.2.8 Plane-wave superposition

Equation (1.23) can be simply interpreted as plane-wave superposition. To make this clear, we first dispose of the *rho* filter by means of a definition.

$$\tilde{u}(p,\tau) \quad = \quad \mathrm{rho}(\tau) * \bar{u}(p,\tau) \tag{10.24}$$

Equation (1.24) will be seen to be more than a definition. We will see that $\tilde{u}(p,\tau)$ can be interpreted as the *plane-wave spectrum* . Substituting the definition (1.24) into both (1.23) and (1.14) gives another transform pair:

$$\boxed{\begin{array}{c} u(x,t) \ = \ \int \tilde{u}(p,t-px)dp \\ \hline \tilde{u}(x,t) \ = \ rho(\tau) \ * \ \int u(x,\tau+px)\ dx \end{array}} \tag{10.25}$$

To confirm that $\tilde{u}(p,\tau)$ may be interpreted as the plane-wave spectrum, we take $\tilde{u}(p,\tau)$ to be the impulse function $\delta(p - p_0)\,\delta(\tau - \tau_0)$ and substitute it into the top half of (1.25). The result $u(x,t) = \delta(t - p_0x - \tau_0)$ is an impulsive plane wave, as expected.

10.2.9 Reflection coefficients—spherical versus planar

The amplitudes that you see on the reflected waves on a field profile are affected by many things. Assume that corrections can be made for the spherical divergence of the wave, the transmission coefficients through the layers, inner bed multiples, etc. What remains are the *spherical-wave reflection coefficients* . Spherical-wave reflection strengths are not the same as the plane-wave reflection coefficients calculated in FGDP or by means of Zoeppritz [1919] equations. Theoretical analyses of reflection coefficient strengths are always based on Fourier analysis. The equations in (1.25) provide a link between plane-wave reflection coefficients and cylindrical-wave reflection coefficients. See page 196 for going from cylinders to spheres.

10.2.10 The rho filter

In practical work, the *rho* filter is often ignored because it can be absorbed into the rest of the filtering effects of the overall data recording and processing activity. However, the *rho* filter is not inconsequential. The integrations in the slant stack enhance low frequencies, and the *rho* filter pushes them back to their appropriate level. Let us inspect this filter. The *rho* filter has the same spectrum as does the time derivative, but their time functions are very different. The finite-difference representation of a time derivative is short, only Δt in time duration. Because of the sharp corner in the absolute-value function, the *rho* filter has a long time duration. The Hilbert kernel $-1/t$ has a Fourier transform $i\,\mathrm{sgn}(\omega)$. Notice that $|\omega| = (-i\omega) \times i\,\mathrm{sgn}(\omega)$. In the time domain this means that $d/dt(-1/t) = 1/t^2$, so $\mathrm{rho}(t) = 1/t^2 + \delta(t)$.

An alternate view is that the *rho* filter should be divided into two parts, with half going into the forward slant stack and the other half into the inverse. Then slant stacking would not cause the power spectrum of the data to change. An interesting way to divide the $|\omega|$ is $|\omega| = \sqrt{-i\omega}\sqrt{i\omega}$. The expression $\sqrt{-i\omega}$ has a causal time function and $\sqrt{i\omega}$ has an anticausal one.

In practice, slant stack is not so cleanly invertible as 2-D FT, so various iteration and optimization techniques are often used.

EXERCISES:

1 Assume that $v(z)$ =const and prove that the width of a Fresnel zone increases in proportion to $\sqrt{t}$.

2 Given $v(z)$, derive the width of the Fresnel zone as a function of t.

10.3 SNELL WAVES AND SKEWED COORDINATES

Slant stacks are closely related to Snell waves. But there is more to it than that. Three different types of gathers (CSP, CGP, and CMP) can be slant stacked, and the meaning is different in each case.

A Snell wave can be synthesized by slant stacking ordinary reflection data. Snell waves are described by wave-propagation theory. You can expect to be able to write a wave equation that really describes the Snell wave despite complexities of lateral velocity variation, multiple reflections, shear waves, or all these complications at once. Contrast this to a CDP stack where downward continuation is already an approximation even when velocity is constant. Of course we can always return to data analysis in shot-geophone space. But the slant stack is a stack, and that means there is already some noise reduction and data compression.

10.3.1 Snell wave information in field data

The superposition principle allows us to create an impulse function by a superposition of sinusoids of all frequencies. A three-dimensional generalization is the creation of a point source by the superposition of plane waves going in all directions. Likewise, a plane wave can be a superposition of many Huygens secondary point sources. A

Snell wave can be simulated by an appropriate superposition, called a *slant stack,* of the point-source data recorded in exploration.

Imagine that all the shots in a seismic survey were shot off at the same time. The downgoing wave would be approximately a plane wave. (Let us ignore the reality that the world is 3-D and not 2-D). The data recorded from such an experiment could readily be simulated from conventional data simply by summing the data field $P(s, g, t)$ over all s. In each common-geophone profile the traces would be summed with no moveout correction.

To simulate a nonvertical Snell wave, successive shots must be delayed (to correspond to a supersonic airplane), according to some prescribed $p_s = dt/ds$.

What happens if data is summed over the geophone axis instead of the shot axis? The result is point-source experiments recorded by receiver antennas that have been highly tuned to receive vertically propagating waves. Time shifting the geophones before summation simulates a receiver antenna that records a Snell wave, say, $p_g = dt/dg$ upcoming at an angle $\sin\theta = p_g v$.

Integration over an axis is an extreme case of low-pass filtering over an axis. Between the two extremes of the point-source case and the plane-wave case is the case of directional senders and receivers.

The simple process of propagation spreads out a point disturbance to a place where, from a distance, the waves appear to be nearly plane waves or Snell waves. Little patches of data where arrivals appear to be planar can be analyzed as though they were Snell waves.

In summary, a *downgoing* Snell wave is achieved by dip filtering in *shot* space, whereas an *upcoming* Snell wave is achieved by dip filtering in *geophone* space.

10.3.2 Muting and data recording

The basic goal of muting is to remove horizontally moving energy. Such energy is unrelated to a deeper image. Typically muting is a weighting function zeroes data generally beyond some value of $(g - s)/t$. There is no question that muting removes much horizontally moving energy, but more can be done. Because of back-scattering, horizontally moving energy can often be found inside the mute zone. The way to get rid of it is to use a dip filter instead of a weighting function. Before modern high-density recording, slow moving noises were often aliased on the geophone cable, so dip filtering wasn't feasible. If the emergent angle isn't close enough to vertical, that is, if dt/dg isn't small enough, then the waves can't have come from the exploration target. On explosion data, filtering is not so easily applied in shot space as it is in geophone space because data is not very densely recorded in shot space. Don't fall into the trap of thinking that this dip filtering can be done on a common-*mid*point gather. Back-scattered ground roll has no moveout on a common-midpoint gather.

Marine water-bottom scatter is frequently so strong that it is poorly suppressed by conventional processing. Earlier we saw the reason: point scatterers imply hyperbolic arrivals, which have steep dip, hence they have the stacking velocities of sediment rather than water. What is needed are two dip filters—one to reject waves leaving the shots at nonpenetrating angles, and the other to reject waves arriving at the geophones at nonpenetrating angles.

Present-day field arrays filter on the basis of spatial frequency k_x. More high-frequency energy would be left in the data if the recording equipment used dip (k/ω) filters instead of spatial-frequency k filters. The causal dip filters described earlier might work nicely.

10.3.3 Synthesizing the Snell wave experiment

Let us synthesize a downgoing Snell wave with field data, then imagine how the upcoming wave will look and how it will carry to us information about the subsurface.

Slant stacking will take the survey line data $P(s, g, t)$, which is a function of shot location s, geophone location g, and travel time t, and sum over the shot dimension, thereby synthesizing the upcoming wave $U(g, t)$, which should have been recorded from a downgoing Snell wave. This should be the case even though there may be lateral velocity variation and multiple reflections.

The summation process is confusing because three different kinds of time are involved:

t	$=$	travel time in the point-source field experiments.
t'	$=$	$t - p(g-s)$ = interpretation time. The shallowest reflectors are seen just after $t' = 0$.
t_{pseudo}	$=$	time in the Snell pseudoexperiment with a moving source.

Time in the pseudoexperiment in a horizontally layered earth has the peculiar characteristic that the further you move out the geophone axis, the later the echoes will arrive. Transform directly from the field experiment time t to interpretation time t' by

$$t' \quad = \quad t_{\text{pseudo}} - px \quad = \quad t - p(g - s) \tag{10.26}$$

Figure 1.11 depicts a downgoing Snell wave.

Figure 1.12 shows a hypothetical common-geophone gather, which could be summed to simulate the Snell wave seen at location g_1 in Figure 1.11. The lateral offset of B from C is identical in Figure 1.11 with that in Figure 1.12 (at two places in Figure 1.12. Repeating the summation for all geophones synthesizes an upcoming wave

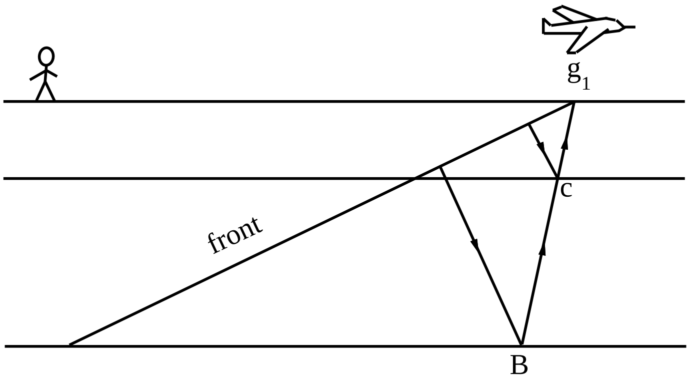

Figure 10.11: Wavefront of a Snell wave that reflects from two layers, carrying information back up to g_1. slnt-snellwave [NR]

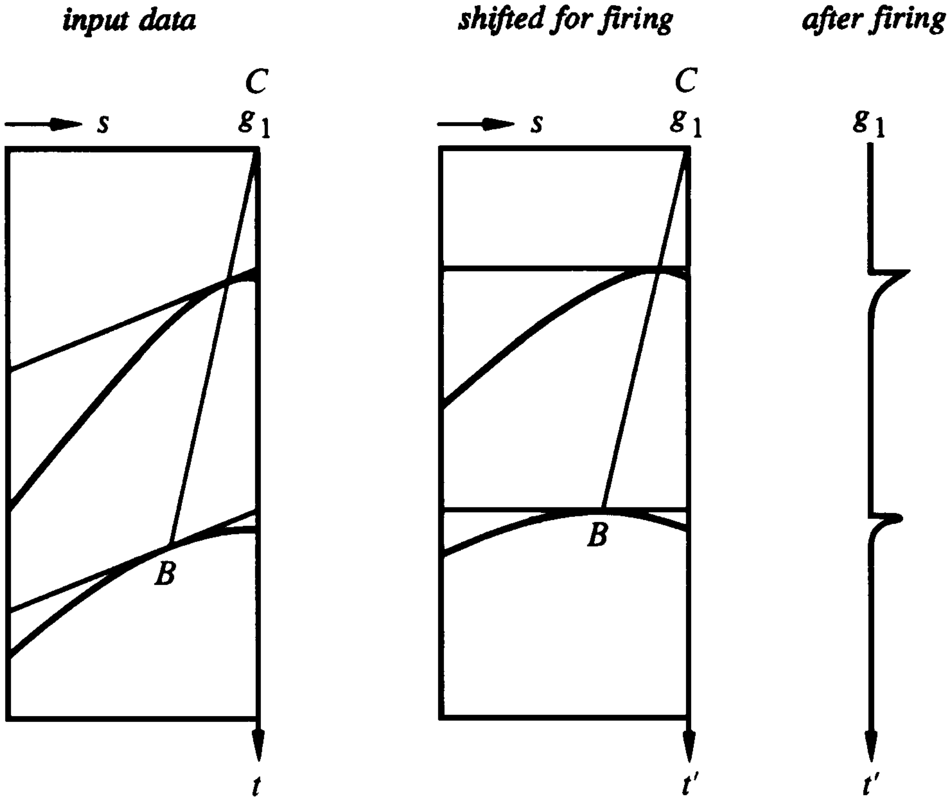

Figure 10.12: On the left is a common-geophone gather at g_1 over two flat reflectors. In the center the data is shifted by linear moveout in preparation for the generation of the synthetic Snell wave by summation over shots. On the right is shown the Snell wave trace recorded at geophone g_1. A Snell wave seismic section consists of many side-by-side traces like g_1. slnt-cspss [NR]

from a downgoing Snell wave.

The variable t' may be called an interpretation coordinate, because shallow reflectors are seen just after $t' = 0$, and horizontal beds give echoes that arrive with no horizontal stepout, unlike the pseudo-Snell wave. For horizontal beds, the detection of lateral location depends upon lateral change in the reflection coefficient. In Figure 1.11, the information about the reflection strength at B is recorded rightward at g_1 instead of being seen above B, where it would be on conventional stack. The moving of received data to an appropriate lateral location is thus an additional requirement for full interpretation.

Figure 1.13 shows the same two flat layers as figures 1 and 2, but there are also anomalous reflection coefficients at points A, B, and C. Point A is directly above point B. The path of the wave reflected at B leads directly to C and thence to g_1. Subsequent frames show the diffraction hyperbolas associated with these three points. Notice that the pseudo-Snell waves reflecting from the flat layers step out at a rate p. Hyperbolas from the scatterers A, B, and C come tangent to the Snell waves at points a, b, and c. Notice that b and c lie directly under g_1 because all are aligned along a raypath with Snell parameter p. The points A, B, and C locate the tops of the hyperbolas since the earliest arrival must be directly above the point scatterer, no matter what the incident wavefield. Converting to the interpretation coordinate t' in the next frame offers the major advantage that arrivals from horizontal layers become horizontal. But notice that the hyperboloids have become skewed. Limiting our attention to the arrivals with little stepout, we find information about the anomalous reflection coefficients entirely in the vicinities of a, b, and c, points which originally lay on hyperbola flanks. These points will not have the correct geometrical location, namely that of A, B and C, until the data is laterally shifted to the left, to, say, $g' = g - f(t')$. Then a will lie above b. The correct amount of shift $f(t')$ is a subject that relates to velocity analysis. The velocity analysis that pertains to this problem will be worked out in the next section.

10.3.4 What's wrong with Snell waves?

Before the DSR was developed, I thought that the only proper way to analyze seismic data was to decompose it into Snell waves. Since a Fresnel zone seems to be about 10° wide, not many Snell waves should be required. The small number of required sections was important because of the limited power of computers in the 1970's. I knew that each Snell wave is analyzable by a single square-root equation, and that even multiple reflections can be handled by methods described in FGDP and in this book. Theoretically this approach was a big improvement over CDP stack, which is hardly analyzable at all. A practical problem for downgoing Snell waves, however, is that they may become complicated early if they encounter lateral velocity inhomogeneity shortly after they depart the earth's surface. I no longer believe that Snell waves are a panacea, although I am unsure what their ultimate role will be. But many waves behave a little like they are Snell waves. This motivates the development

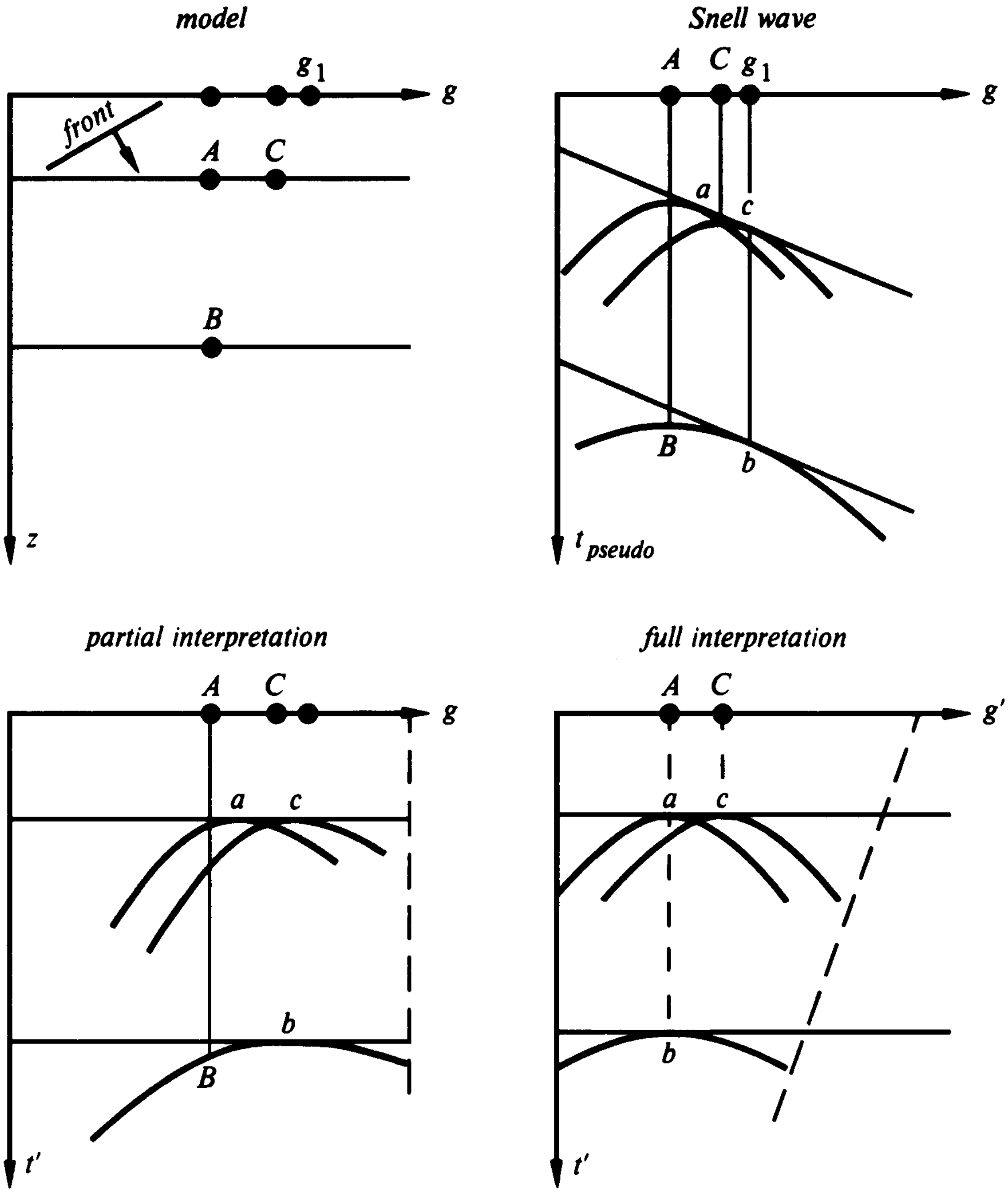

Figure 10.13: Top left is three point scatterers on two reflectors. Top right is the expected Snell wave. Bottom left is the Snell wave after linear moveout. Bottom right is after transform to full interpretation coordinates. At last a, b, and c are located where A, B, and C began. slnt-interpcoord [NR]

of a coordinate system that is ideal for Snell waves, and good for waves that are not far from being Snell waves.

10.3.5 Lateral invariance

The nice thing about a vertically incident source of plane waves $p = 0$ in a horizontally stratified medium is that the ensuing wavefield is laterally invariant. In other words, an observation or a theory for a wavefield would in this case be of the form $P(t) \times \mathrm{const}(x)$. Snell waves for any particular nonzero p-value are also laterally invariant. That is, with

$$t' = t - px \tag{10.27}$$
$$x' = x \tag{10.28}$$

lateral invariance is given by the statement

$$P(x,t) = P'(t') \times \mathrm{const}(x') \tag{10.29}$$

Obviously, when an apparently two-dimensional problem can be reduced to one dimension, great conceptual advantages result, to say nothing of sampling and computational advantages. Before proceeding, study equation (1.29) until you realize why the wavefield can vary with x but be a constant function of x' when (1.28) says $x = x'$.

The coordinate system (1.27) and (1.28) is a retarded coordinate system, not a moving coordinate system. Moving coordinate systems work out badly in solid-earth geophysics. The velocity function is never time-variable in the earth, but it becomes time-variable in a moving coordinate system. This adds a whole dimension to computational complexity.

The goal is to create images from data using a *model* velocity that is a function of all space dimensions. But the coordinate system used will have a *reference* velocity that is a function of depth only.

10.3.6 Snell wave coordinates

A Snell wave has three intrinsic planes, which suggests a coordinate system. First are the layer planes of constant z, which include the earth's surface. Second is the plane of rays. Third is the moving plane of the wavefront. The planes become curved when velocity varies with depth.

The following equations define *Snell wave coordinates:*

$$z'(z,x,t) = z\,\frac{\cos\theta}{v} \tag{10.30}$$
$$x'(z,x,t) = z\,\tan\theta + x \tag{10.31}$$
$$t'(z,x,t) = z\,\frac{\cos\theta}{v} - x\,\frac{\sin\theta}{v} + t \tag{10.32}$$

Equation (1.30) simply defines a travel-time depth using the vertical phase velocity seen in a borehole. Interfaces within the earth are just planes of constant z'.

Setting x' as defined by equation (1.31) equal to a constant, say, x_0, gives the equation of a ray, namely, $(x - x_0)/z = -\tan\theta$. Different values of x_0 are different rays.

Setting t' as defined by equation (1.32) equal to a constant gives the equation for a moving wavefront. To see this, set $t' = t_0$ and note that at constant x you see the borehole speed, and at constant z you see the airplane speed.

Mathematically, one equation in three unknowns defines a plane. So, setting the left side of any of the equations (4a,b,c) to a constant gives an equation defining a plane in (z, x, t)-space. To get some practice, we will look at the intersection of two planes. Staying on a wavefront requires $dt' = 0$. Using equation (1.32) gives

$$dt' \quad = \quad 0 \quad = \quad \frac{\cos\,\theta}{v}\,dz \;-\; \frac{\sin\,\theta}{v}\,dx \;+\; dt \tag{10.33}$$

Combining the constant wavefront equation $dt' = 0$ with the constant depth equation $dz' = dz = 0$ gives the familiar relationship

$$\frac{dt}{dx} \quad = \quad p \tag{10.34}$$

When coordinate planes are nonorthogonal, the coordinate system is said to be *affine.* With affine coordinates, such as (1.30), (1.31) and (1.32), we have no problem with computational tractability, but we often do have a problem with our own confusion. For example, when we display movies of marine field data, we see a sequence of (h, t)-planes. Successive planes are successive shot points. So the data is displayed in (s, h) when we tend to think in the orthogonal coordinates (y, h) or (s, g). With affine coordinates I find it easiest to forget about the coordinate axis, and think instead about the perpendicular plane. The shot axis $\mathbf{s}$ can be thought of as a plane of constant geophone, say, cg. So I think of the marine-data movie as being in (cs, ch, ct)-space. In this movie, another plane, really a family of planes, the planes of constant midpoints cy, sweep across the screen, along with the "texture" of the data.

To define Snell coordinates when the velocity is depth-variable, it is only necessary to interpret (1.30), (1.31) and (1.32) carefully. First, all angles must be expressed in terms of p by the Snell substitution $\sin\theta = pv(z)$. Then z must everywhere be replaced by the integral with respect to z.

10.3.7 Snell Waves in Fourier space

The chain rule for partial differentiation says that

$$\begin{bmatrix} \partial_t \\ \partial_x \\ \partial_z \end{bmatrix} \quad = \quad \begin{bmatrix} {t'}_t & {x'}_t & {z'}_t \\ {t'}_x & {x'}_x & {z'}_x \\ {t'}_z & {x'}_z & {z'}_z \end{bmatrix} \begin{bmatrix} \partial_{t'} \\ \partial_{x'} \\ \partial_{z'} \end{bmatrix} \tag{10.35}$$

In Fourier space, the top two rows of the above matrix may be interpreted as

$$-i\,\omega \quad = \quad -i\,\omega' \tag{10.36}$$

$$i\,k_x \quad = \quad +p\,\omega' \;+\; i\,k'_x \tag{10.37}$$

Of particular interest is the energy that is flat after linear moveout (constant with x'). For such energy $\partial/\partial x' = ik'_x = 0$. Combining (1.36) and (1.37) gives the familiar equation

$$p \quad = \quad \frac{k}{\omega} \tag{10.38}$$

EXERCISES:

1 Explain the choice of sign of the s-axis in Figure 1.11.

2 Equations (1.30), (1.31) and (1.32) are for *upgoing* Snell waves. What coordinate system would be appropriate for *downgoing* Snell waves?

3 Express the scalar wave equation in the coordinate system (1.30), (1.31) and (1.32). Neglect first derivatives.

4 Express the dispersion relation of the scalar wave equation in terms of the Fourier variables (ω', k'_x, k'_z).

10.4 INTERVAL VELOCITY BY LINEAR MOVEOUT

Linear moveout forms the basis for a simple, graphical method for finding seismic velocity. The method is particularly useful for the analysis of data that is no longer in a computer, but just exists on a piece of paper. Additionally, the method offers insights beyond those offered by the usual computerized hyperbola scan. Using it will help us rid ourselves of the notion that angles should be measured from the vertical ray. Non-zero Snell parameter can be the "default."

Ultimately this method leads to a definition of *velocity spectrum,* a plane in which the layout of data, after a linear invertible transformation, shows the seismic velocity.

10.4.1 Graphical method for interval velocity measurement

A wave of velocity v from a point source at location $(x, z) = (0, z_s)$ passes any point (x, z) at time t where

$$v^2\,t^2 \quad = \quad x^2 \;+\; (z \;-\; z_s)^2 \tag{10.39}$$

In equation (1.39) x should be replaced by either half-offset h or midpoint y. Then t is two-way travel time; the velocity v is half the rock velocity; and $(z \;-\; z_s)$ is the distance to an image source.

Differentiating (1.39) with respect to t (at constant z) gives

$$v^2 \; 2 \; t \quad = \quad 2 \; x \; \frac{dx}{dt} \tag{10.40}$$

$$v^2 \quad = \quad \frac{x}{t} \; \frac{dx}{dt} \tag{10.41}$$

Figure 1.14 shows that the three parameters required by (1.41) to compute the material velocity are readily measured on a common-midpoint gather.

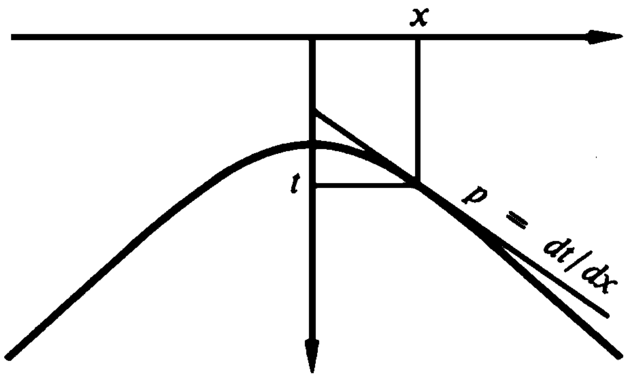

Figure 10.14: A straight line, drawn tangent to hyperbolic observations. The slope p of the line is arbitrary and may be chosen so that the tangency occurs at a place where signal-to-noise ratio is good. (Gonzalez) slnt-tangent [NR]

Equation (1.41) can be used to estimate a velocity whether or not the earth really has a constant velocity. When the earth velocity is stratified, say, $v(z)$, it is easy to establish that the estimate (1.41) is exactly the root-mean-square (RMS) velocity. First recall that the bit of energy arriving at the point of tangency propagates throughout its entire trip with a constant Snell parameter $p = dt/dx$.

The best way to specify velocity in a stratified earth is to give it as some function $v'(z)$. Another way is to pick a Snell parameter p and start descending into the earth on a ray with this p. As the ray goes into the earth from the surface $z = 0$ at $t = 0$, the ray will be moving with a speed of, say, $v(p,t)$. It is an elementary exercise to compute $v(p,t)$ from $v'(z)$ and vice versa. The horizontal distance x which a ray will travel in time t is given by the time integral of the horizontal component of velocity, namely,

$$x \quad = \quad \int_0^t v(p,t) \; \sin \theta \; dt \tag{10.42}$$

Replacing $\sin \theta$ by pv and taking the constant p out of the integral yields

$$x \quad = \quad p \int_0^t v(p,t)^2 \; dt \tag{10.43}$$

Recalling that $p = dt/dx$, recopy (1.41) and insert (1.43):

$$v^2_{\text{measured}} \quad = \quad \frac{x}{t} \; \frac{dx}{dt} \tag{10.44}$$

$$v^2_{\text{measured}} \quad = \quad \frac{1}{t} \int_0^t v(p,t)^2 \; dt \tag{10.45}$$

which justifies the assertion that

$$v_{\text{measured}} \quad = \quad v_{\text{root-mean-square}} \quad = \quad v_{\text{RMS}} \tag{10.46}$$

Equation (1.45) is exact. It does not involve a "small offset" assumption or a "straight ray" assumption.

Next compute the *interval* velocity. Figure 1.15 shows hyperboloidal arrivals from two flat layers. Two straight lines are constructed to have the same slope p. Then

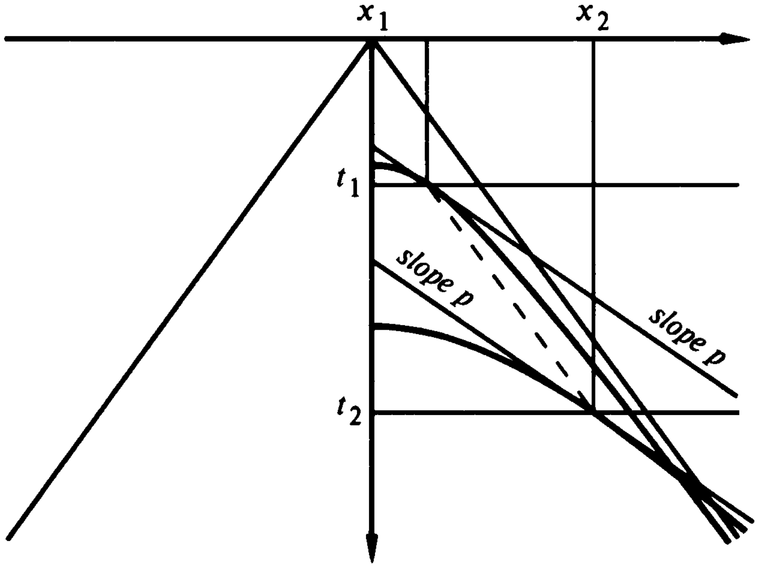

Figure 10.15: Construction of two parallel lines on a common-midpoint gather which are tangent to reflections from two plane layers. (Gonzalez) slnt-tan2 [NR]

the tangencies are measured to have locations (x_1, t_1) and (x_2, t_2). Combining (1.44) with (1.42), and using the subscript j to denote the j^{th} tangency (x_j, t_j), gives

$$x_j \, \frac{dx}{dt} \quad = \quad \int_0^{t_j} \; v(p,t)^2 \; dt \tag{10.47}$$

Assume that the velocity between successive events is a constant v_{interval}, and subtract (1.47) with $j+1$ from (1.47) with j to get

$$(x_{j+1} \; - \; x_j) \, \frac{dx}{dt} \quad = \quad (t_{j+1} \; - \; t_j) \; v_{\text{interval}}^2 \tag{10.48}$$

Solving for the interval velocity gives

$$v_{\text{interval}}^2 \quad = \quad \frac{x_{j+1} \; - \; x_j}{t_{j+1} \; - \; t_j} \, \frac{dx}{dt} \tag{10.49}$$

So the velocity of the material between the j^{th} and the $j+1^{\text{st}}$ reflectors can be measured directly using the square root of the product of the two slopes in (1.49), which are the dashed and solid straight lines in Figure 1.15. The advantage of manually placing straight lines on the data, over automated analysis, is that you can graphically visualize the noise sensitivity of the measurement, and you can select on the data the best offsets at which to make the measurement.

If you do this routinely you quickly discover that the major part of the effort is in accurately constructing two lines that are tangent to the events. When you run into difficulty, you will find it convenient to replot the data with linear moveout $t' = t - px$. After replotting, the lines are no longer sloped but horizontal, so that any of the many timing lines can be used. Locating tangencies is now a question of finding the tops of convex events. This is shown in Figure 1.16.

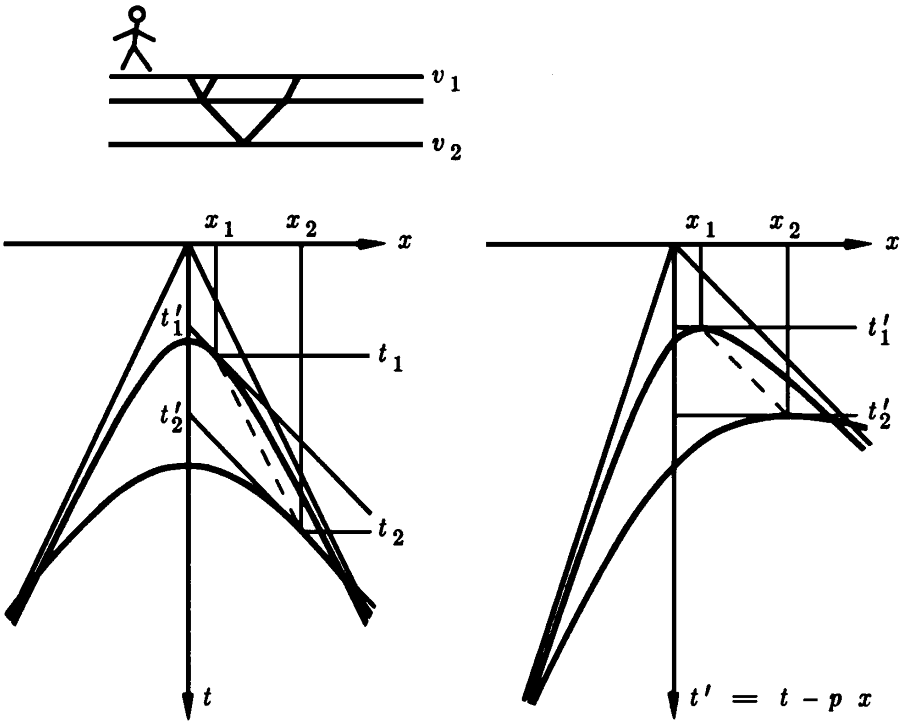

Figure 10.16: Measurement of interval velocity by linear moveout. (Gonzalez) slnt-tan3 [NR]

In terms of the time t', equation (1.49) is

$$v^2_{\text{interval}} \quad = \quad \frac{1}{\frac{\Delta t}{\Delta x}} \, \frac{1}{p} \quad = \quad \frac{1}{\frac{\Delta t'}{\Delta x} \; + \; p} \, \frac{1}{p} \tag{10.50}$$

Earth velocity is measured on the right side of Figure 1.16 by measuring the slope of the dashed line, namely $\Delta t'/\Delta x$, and inserting it into equation (1.50). (The value of p is already known by the amount of linear moveout that was used to make the plot).

10.4.2 Common-midpoint Snell coordinates

Common-*midpoint* slanted wave analysis is a more conservative approach to seismic data analysis than the Snell wave approach. The advantage of common-midpoint analysis is that the effects of earth dip tend to show up mainly on the midpoint axis, and the effect of seismic velocity shows up mainly on the offset axis. Our immediate goal is to define an invertible, wave-equation approach to determination of interval velocity.

The disadvantage of common-midpoint analysis is that it is nonphysical. A slant stack at common geophone simulates a downgoing Snell wave, and you expect to be able to write a differential equation to describe it, no matter what ensues, be it multiple reflection or lateral velocity variation. A common-*midpoint* slant stack does not model anything that is physically realizable. Nothing says that a partial differential equation exists to extrapolate such a stack. This doesn't mean that there is necessarily anything wrong with a common-midpoint *coordinate* system. But it does make us respect the Snell wave approach even though its use in the industrial world is not exactly growing by leaps and bounds.

(Someone implementing common-midpoint slant stack would immediately notice that it is easier than slant stack on common-geophone data. This is because at a common midpoint, the tops of hyperboloids must be at zero offset, the location of the Fresnel zone is more predictable, and interpolation and missing data problems are much alleviated).

Seismic data is collected in time, geophone, shot, and depth coordinates (t, g, s, z). A new four-component system will now be defined. Midpoint is defined in the usual way:

$$y(t,g,s,z) \quad = \quad \frac{g \ + \ s}{2} \tag{10.51}$$

Travel-time depth is defined using the vertical phase velocity in a borehole. Two-way travel times are used, in order to be as conventional as possible:

$$\tau(t,g,s,z) \quad = \quad 2\ z\ \frac{\cos\theta}{v} \tag{10.52}$$

Next the surface offset h' is defined. We will not use the old definition of offset. For this method, shots and geophones should not go straight down, but along a ray. This can be so if h' is defined as follows:

$$h'(t,g,s,z) \quad = \quad \frac{g \ - \ s}{2} \ + \ z \tan\theta \tag{10.53}$$

With this new definition of h' the separation of the shot and geophone decreases with depth for constant h'.

Define the *LMO time* as the travel time in the point-source experiment less the linear moveout. So, at any depth, the LMO time is $t \ - \ p(g-s)$. As h' was defined to be the *surface* half-offset, t' is defined to be the *surface* LMO time. From the LMO time of a buried experiment, the LMO time at the surface is defined by adding in the travel-time depth of the experiment:

$$t' \quad = \quad t \ - \ p(g \ - \ s) \ + \ \tau \tag{10.54}$$

You may like to think of (1.54) as a "slant" on time retardation for upcoming waves, say, $t' \ = t_{\mathrm{LMO}} + z_{\mathrm{slant}}/v$. Formally,

$$t'(t,g,s,z) \quad = \quad t \ - \ p(g \ - \ s) \ + \ 2 \ z \ \frac{\cos\,\theta}{v} \tag{10.55}$$

Figure 1.17 is a geometrical representation of these concepts.

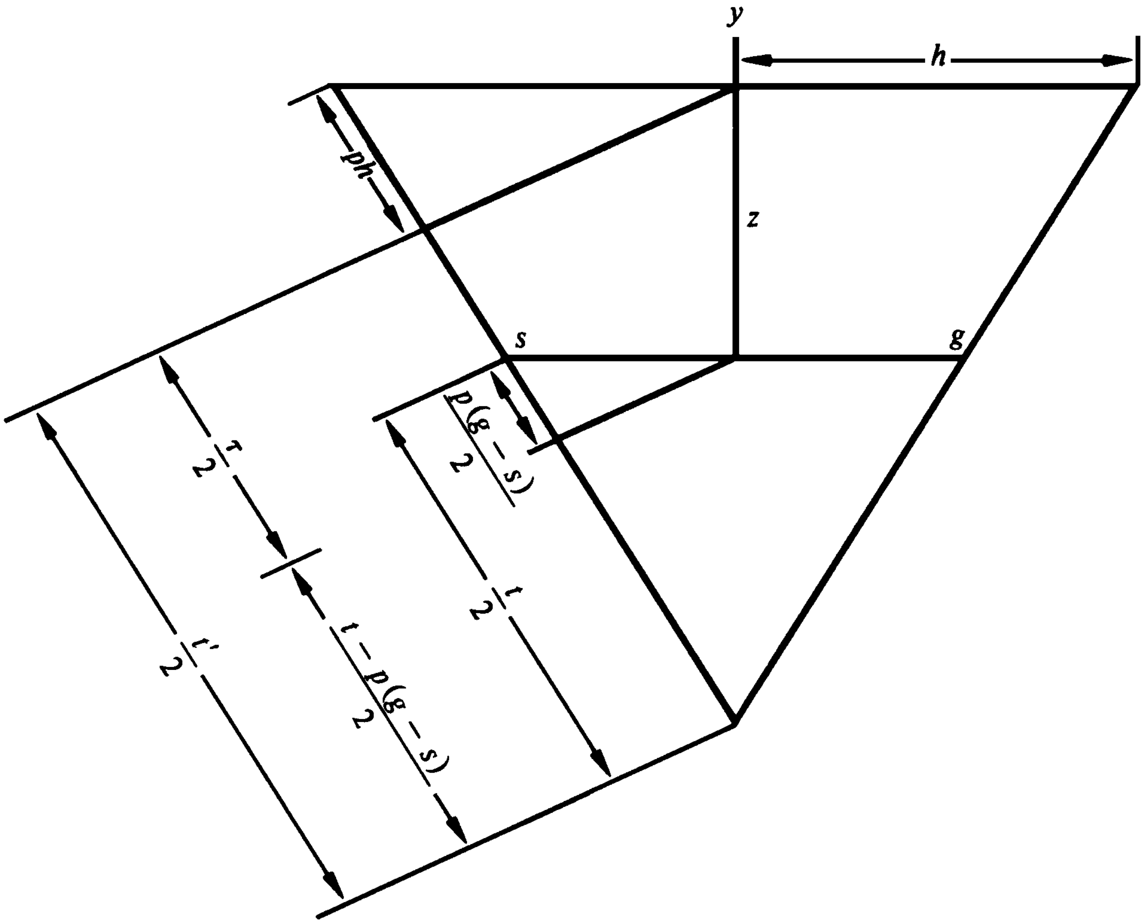

Figure 10.17: The CMP-LMO coordinate frame geometry. This is a natural coordinate system for describing waves that resemble a reference Snell wave. slnt-cmplmo [NR]

From the geometry of Figure 1.17 it will be deduced that a measurement of a reflection at some particular value of (h', t') directly determines the velocity. Write an equation for the reflector depth:

$$v \ \left(\frac{t'}{2} \ + \ p\,h'\right) \ \cos\,\theta \quad = \quad \text{reflector depth} \quad = \quad \frac{h'}{\tan\,\theta} \tag{10.56}$$

Using Snell's law to eliminate angles and solving for velocity gives

$$v^2 \quad = \quad \frac{1}{p} \ \frac{1}{p \ + \ \frac{t'}{2h'}} \tag{10.57}$$

This is consistent with equation (1.50).

Gathering the above definitions into a group, and allowing for depth-variable velocity by replacing z by the integral over z, we get

$$t'(t,g,s,z) \quad = \quad t \ - \ p(g \ - \ s) \ + \ 2 \int_0^z \frac{\cos \ \theta}{v} \ dz \tag{10.58}$$

$$y(t,g,s,z) \quad = \quad \frac{g \ + \ s}{2} \tag{10.59}$$

$$h'(t,g,s,z) \quad = \quad \frac{g \ - \ s}{2} \ + \ \int_0^z \tan \ \theta \ dz \tag{10.60}$$

$$\tau(t,g,s,z) \quad = \quad 2 \int_0^z \frac{\cos \ \theta}{v} \ dz \tag{10.61}$$

Before these equations are used, all the trigonometric functions must be eliminated by Snell's law for stratified media, $\sin\theta(z) = pv(z)$. Snell's parameter p is a numerical constant throughout the analysis.

The equation for interval velocity determination (1.50) again arises when dt'/dz from (1.58) and dh'/dz from (1.60) are combined:

$$\frac{dt'}{dh'} \quad = \quad \frac{2 \ \cos \theta}{v \ \tan \theta} \tag{10.62}$$

Eliminating the trig functions with $p\,v \ = \ \sin\theta$ allows us to solve for the interval velocity:

$$v^2 \quad = \quad \frac{1}{p} \frac{1}{p \ + \ \frac{1}{2}\frac{dt'}{dh'}} \tag{10.63}$$

At the earth's surface $z = 0$, seismic survey data can be put into the coordinate frame (1.58), (1.59), (1.60), and (1.61) merely by making a numerical choice of p and doing the linear moveout. No knowledge of velocity $v(z)$ is required so far. Then we look at the data for some tops of the skewed hyperbolas. Finding some, we use equation (1.50), (1.57) or (1.63) to get a velocity with which to begin downward continuation.

Waves can be described in either the (t,g,s,z) physical coordinates or the newly defined coordinates (t',y,h',τ). In physical coordinates the image is found at

$$t \quad = \quad 0 \qquad \text{and} \qquad g \quad = \quad s \tag{10.64}$$

To express these conditions in the Snell coordinates, insert (1.64) into (1.58) and (1.61). The result is what programmers call the stopping condition:

$$t' \quad = \quad \tau \tag{10.65}$$

This is the depth at which the velocity information should be best focused in the (h',t')-plane. Next some downward-continuation equations.

10.4.3 Differential equations and Fourier transforms

The chain rule for partial differentiation gives

$$\begin{bmatrix} \partial_t \\ \partial_g \\ \partial_s \\ \partial_z \end{bmatrix} = \begin{bmatrix} t'_t & y_t & h'_t & \tau_t \\ t'_g & y_g & h'_g & \tau_g \\ t'_s & y_s & h'_s & \tau_s \\ t'_z & y_z & h'_z & \tau_z \end{bmatrix} \begin{bmatrix} \partial_{t'} \\ \partial_y \\ \partial_{h'} \\ \partial_\tau \end{bmatrix} \tag{10.66}$$

In our usual notation the Fourier representation of the time derivative ∂_t is $-i\omega$. Likewise, $\partial_{t'}$ and the spatial derivatives $(\partial_y, \partial_{h'}, \partial_\tau,\ \partial_g, \partial_s, \partial_z)$ are associated with $i(k_y, k_{h'}, k_\tau,\ k_g, k_s, k_z)$. Using these Fourier variables in the vectors of (1.66) and differentiating (1.58), (1.59), (1.60), and (1.61) to find the indicated elements in the matrix of (1.66), we get

$$\begin{bmatrix} 1 & 0 & 0 & 0 \\ -p & \frac{1}{2} & \frac{1}{2} & 0 \\ p & \frac{1}{2} & -\frac{1}{2} & 0 \\ \frac{2\cos\theta}{v} & 0 & \tan\theta & \frac{2\cos\theta}{v} \end{bmatrix} = \begin{bmatrix} 1 & 0 & 0 & 0 \\ -p & \frac{1}{2} & \frac{1}{2} & 0 \\ p & \frac{1}{2} & -\frac{1}{2} & 0 \\ \frac{2\cos\theta}{v} & 0 & \tan\theta & \frac{2\cos\theta}{v} \end{bmatrix} \begin{bmatrix} -\omega' \\ k_y \\ k_{h'} \\ k_\tau \end{bmatrix} \tag{10.67}$$

Let S be the sine of the takeoff angle at the source and let G be the sine of the emergent angle at the geophone. If the velocity v is known, then these angles will be directly measurable as stepouts on common-geophone gathers and common-shot gathers. Likewise, on a constant-offset section or a slant stack, observed stepouts relate to an apparent dip Y, and on a linearly moved-out common-midpoint gather, stepouts measure the apparent stepout H'. The precise definitions are

$$S = \frac{v\,k_s}{\omega} \qquad\qquad G = \frac{v\,k_g}{\omega} \tag{10.68}$$

$$Y = \frac{v\,k_y}{2\,\omega} \qquad\qquad H' = \frac{v\,k_{h'}}{2\,\omega} \tag{10.69}$$

With these definitions the second and third rows of (1.67) become

$$G = p\,v + Y + H' = Y + (H' + p\,v) \tag{10.70}$$

$$S = -p\,v + Y - H' = Y - (H' + p\,v) \tag{10.71}$$

The familiar offset stepout angle H is related to the LMO residual stepout angle H' by $H' = H - pv$. Setting H' equal to zero means setting $k_{h'}$ equal to zero, thereby indicating integration over h', which in turn indicates slant stacking data with slant angle p. Small values of H'/v or $k_{h'}/\omega$ refer to stepouts near to p.

10.4.4 Processing possibilities

The double-square-root equation is

$$\frac{k_z}{\omega} = -\frac{1}{v}\left(\sqrt{1 - S^2} + \sqrt{1 - G^2} \right) \tag{10.72}$$

With substitutions of the first and fourth rows of (1.67), and (1.68) the DSR equation becomes

$$\frac{k_\tau}{\omega} = 1 - \frac{pv}{1 - p^2v^2} H' - \frac{1}{2} \left(\sqrt{1 - \frac{2pv(H' - Y) + (H' - Y)^2}{1 - p^2v^2}} \right.$$
$$\left. + \sqrt{1 - \frac{2pv(H' + Y) + (H' + Y)^2}{1 - p^2v^2}} \right) \tag{10.73}$$

Equation (1.73) is an exact representation of the double-square-root equation in what is called *retarded Snell midpoint coordinates.*

The coordinate system (1.58), (1.59), (1.60), and (1.61) can describe any wavefield in any medium. It is is particularly advantageous, however, only in stratified media of velocity near $v(z)$ for rays that are roughly parallel to any ray with the chosen Snell parameter p. There is little reason to use these coordinates unless they "fit" the wave being studied. Waves that fit are those that are near the chosen p value. This means that H' doesn't get too big. A variety of simplifying expansions of (1.73) are possible. There are many permutations of magnitude inequalities among the three ingredients pv, H', and Y. You will choose the expansion according to the circumstances. The appropriate expansions and production considerations, however, have not yet been fully delineated. But let us take a look at two possibilities.

First, any dataset can be decomposed by stepout into many datasets, each with a narrow bandwidth in stepout space—CMP slant stacks, for example. For any of these datasets, H' could be ignored altogether. Then (1.73) would reduce to

$$\frac{k_\tau}{\omega} = 1 - \frac{1}{2} \left(\sqrt{1 - \frac{-2pvY + Y^2}{1 - p^2v^2}} + \sqrt{1 - \frac{+2pvY + Y^2}{1 - p^2v^2}} \right) \tag{10.74}$$

or

$$\frac{k_\tau}{\omega} = 1 - \frac{1}{2\sqrt{1 - p^2v^2}} \left[\sqrt{1 - (Y - pv)^2} + \sqrt{1 - (Y + pv)^2} \right] \tag{10.75}$$

The above approach is similar to the one employed by Richard Ottolini in his dissertation.

Next, let us make up an approximation to (1.73) which is separable in Y and H'. Equation (1.75) provides the first part. Then take $Y = 0$ and keep *all* terms up to quadratics in H':

$$\frac{k_\tau}{\omega} = \frac{H'^2}{2(1 - p^2v^2)^2} \tag{10.76}$$

A separable approximation of (1.73) is (1.75) plus (1.76). It is no accident that there are no linear powers of H' in (1.76). The coordinate system was designed so that energy near the chosen model $Y = 0$ and $H = pv$ should not drift in the (h', t')-plane as the downward continuation proceeds.

The velocity spectrum idea represented by equation (1.76) is to use the H' term to focus the data on the (h', t')-plane. After focusing, it should be possible to read interval velocities directly as slopes connecting events on the gathers. This approach was used in the dissertation of Alfonso Gonzalez [1982].

EXERCISES:

1 A hyperbola is identified on a zero-offset section. The top is obscured but you can measure (p, x, t) at two places. What is the earth velocity? Given the same measurements on a field profile (constant s) what is the earth velocity?